TECHNICAL TRANSACTIONS | CZASOPISMO TECHNICZNE
CIVIL ENGINEERING | BUDOWNICTWO
2-B/2015

YASUSHI UEMATSU[*], YOSHIKI SHIMIZU[**],
YOSHIMASA MIYAKE[***], YUSUKE KANEGAE[***]

WIND-INDUCED SCATTERING OF PERMEABLE UNIT FLOORING DECKS LOOSELY LAID ON ROOFTOPS AND BALCONIES OF HIGH-RISE BUILDINGS

PODRYWANIE PRZEZ WIATR NIEZAMOCOWANYCH PODESTÓW TARASOWYCH UKŁADANYCH NA BALKONACH I DACHACH BUDYNKÓW WYSOKICH

Abstract

The present paper discusses the mechanism of the wind-induced scattering of permeable unit flooring decks loosely laid on the rooftops and balconies of high-rise buildings. Firstly, the scattering mechanism of decks was investigated, based on a blowing test using a blower and actual decks. Subsequently, a simulation model was constructed for estimating the internal pressures under the decks (pressures acting on the bottom surface of decks) obtained from a wind tunnel experiment – this is based upon the unsteady Bernoulli equation and the time history of external pressures on the rooftop and balconies. Combining the simulated internal pressures and the experimentally obtained external pressures, the time history of net wind pressures acting on the decks were computed. Finally, the threshold wind speed of scattering (scattering wind speed) was obtained by applying the scattering mechanism to the simulated time history of the net wind pressures.

Keywords: scattering, permeable deck, numerical simulation, wind tunnel experiment, high-rise building, rooftop, balcony

Streszczenie

W niniejszej pracy omówiono mechanizm rozwiewania przez wiatr przepuszczalnych podestów tarasowych luźno ułożonych na dachach i balkonach wieżowców. W pierwszym etapie przeanalizowano mechanizm rozwiewania podestów przy użyciu dmuchawy i rzeczywistych podestów. Następnie zbudowano model symulacyjny do szacowania ciśnienia wewnętrznego na podesty (ciśnienie działające na dolną powierzchnię podestów). Model oparto na nieustalonym równaniu Bernoulliego i przebiegach czasowych ciśnienia zewnętrznego działającego na dach i balkony, które zostały otrzymane w ramach eksperymentu przeprowadzonego w tunelu aerodynamicznym. Na podstawie symulowanych ciśnień wewnętrznych i uzyskanych doświadczalnie ciśnień zewnętrznych, obliczono przebieg czasowy całkowitych ciśnień działających na podesty. W ostatnim etapie obliczono progową prędkość wiatru podczas rozwiewania (prędkość rozwiewania) przez zastosowanie mechanizmu rozwiewania do symulowanych przebiegów czasowych ciśnienia wiatru.

Słowa kluczowe: rozwiewanie, podesty przepuszczające wiatr, symulacje numeryczne, badania w tunelu aerodynamicznym, budynki wysokie, dach, balkon.

DOI: 10.4467/2353737XCT.15.132.4169

[*] Department of Architecture and Building Science, Tohoku University, Japan.
[**] Design Division, Shimizu Corporation, Japan.
[***] Technology Department, Tokyo Plant, Sekisui Chemical Co., Ltd, Japan.

1. Introduction

Permeable unit flooring decks, as shown in Fig. 1a, are often laid on the rooftops and balconies of high-rise buildings (see Fig. 1b). Because such decks are usually just put on (not fixed to) the floors, they are easily blown off by strong winds; this may cause damage to other buildings and people. Because the decks have holes or slits, the internal pressures underneath the decks (i.e. pressures acting on the bottom surface of the decks) depend on their permeability as well as on the external pressures. It is quite difficult to measure the internal pressures directly in a wind tunnel experiment with reduced scale models, because the length L and gap g between the deck and the floor is very small, such as $L \approx 300$ mm and $g \approx 15$ mm, for example. By comparison, it is relatively easy to measure the external pressures on the rooftops and balconies in a wind tunnel experiment. The results can be used for evaluating the internal pressures by using a numerical simulation.

a) b)

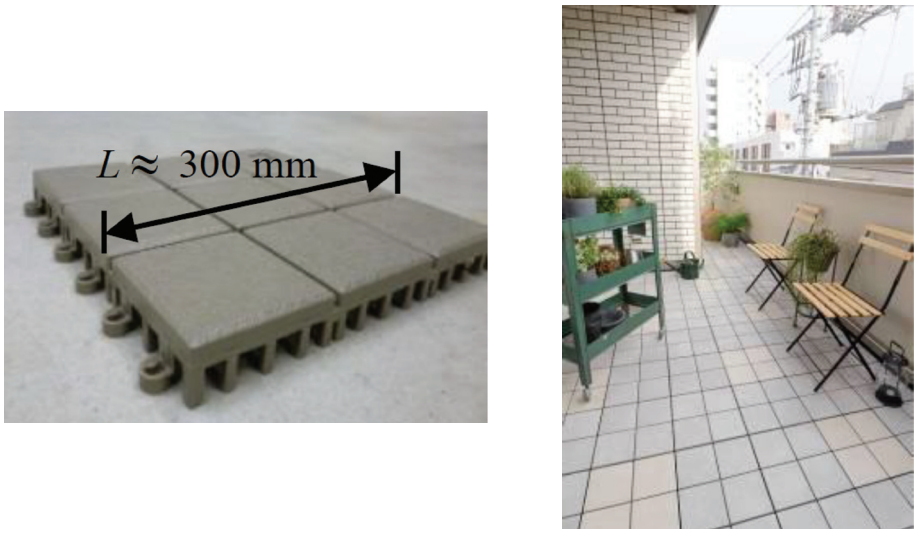

Fig. 1. Permeable unit flooring decks, a) sample, b) unit flooring decks loosely laid on balcony floor (example)

Wind loads on permeable materials placed on the external surfaces of buildings have been studied by many researchers. For example, Cheung and Melbourne [5] measured the net wind pressures acting on porous roofs with a number of small circular holes uniformly distributed over the roof area in a wind tunnel – this showed a significant reduction of the wind forces due to pressure equalization. The effects of porosity and internal volume on the wind load reduction were qualified for a wind direction normal to a wall of the building. A similar problem was numerically studied by Trung et al. [17]. Loose-laid concrete blocks are often used for roof-insulation systems on flat-roofed buildings. Because the blocks

are held in place by gravity, they may be blown off by strong winds. Kind and Wardlaw [9] investigated the mechanism responsible for wind damage to loose-laid roof-insulation systems in a large wind tunnel. They focused on the uplift produced by the differences in static pressure between the exterior and under-surfaces of the block. In the wind resistant design of such decks, it is important to predict the net wind pressures acting upon them. The pressure in the cavity underneath the deck depends on many factors, such as external pressures at the openings and wind permeability and resistance at the gaps. Bienkiewicz and Sun [3, 4] discussed the wind loading on and wind resistance of loose-laid roof paver systems on a low-rise flat-roofed building based on a wind tunnel experiment. They focused on a cornering wind of 45^{o} that causes high levels of suctions near the windward corner. An analytical model for predicting the cavity pressures was proposed by Amano et al. [1], which was an extension of the analytical model proposed by Liu and Saathoff [12]. They used the unsteady discharge equation for flows in the cavity between the layers, perceiving the cavity flow as the orifice flow. The analytical model was validated by a comparison with a wind tunnel experiment. Oh and Kopp [15] developed an analytical model to simulate time-varying pressure distributions in the cavity of air-permeable, double-layer roof systems. The simulated results were found to strongly agree with the wind tunnel results for a low-rise flat-roofed building. Mooneghi et al. [13] made a large scale testing on the wind uplift of roof pavers, in which both wind blow-off tests and pressure measurements were carried out on a square portion of a flat roof for the critical wind direction that generates conical vortices. Most of the previous studies, including the above-mentioned studies, focused on loose-laid roof paver systems placed on the rooftops of low-rise flat-roofed buildings. The blocks are usually made of concrete, and are consequently relatively heavy. Okada et al [16] developed an analytical method for predicting the wind pressures under roof tiles laid on a gable roof, based on the model proposed by Oh et al. [14]. They carried out full-scale measurements, the results of which agreed relatively well with the predicted results.

Besides the roofing systems, wind loads on permeable materials, such as facades, rainscreen walls and siding, have been studied by many researchers [6, 7, 11].

The objective of the present study is to propose a procedure for predicting the threshold wind speed that causes the scattering of permeable unit flooring decks loosely laid on the rooftops and balconies of high-rise buildings. The unit flooring decks under consideration are generally small and light compared with the roof pavers that were investigated in the previous studies. Therefore, they may be blown off by strong winds more easily. Furthermore, the decks are often laid on the balconies of high-rise apartment buildings (see Fig. 1b). To the authors' best knowledge, no study has been conducted on the scattering of unit flooring decks from the balconies of high-rise buildings.

The present paper is divided into three main parts. Firstly, a wind blow-off test using a blower and actual flooring decks is conducted to investigate the scattering mechanism. The distribution of net wind pressure (pressure difference) on the decks is also measured. A discussion is made of the condition that causes the scattering of decks based on a balance of moments caused by the deadweight of and the wind force on the deck. In this test, the flow around decks under practical conditions is not necessarily simulated. The main purpose of this experiment is not to predict the scattering wind speeds under practical conditions but to understand the fundamental mechanism that causes the scattering of decks. Secondly, a numerical simulation model for evaluating the internal pressures underneath the decks is constructed based on the unsteady Bernoulli equations and the time history of external

pressures obtained from a wind tunnel test. The simulation model is based on those proposed by Oh et al. [14] and Okada et al.[16]. A tuning of the parameters involved in the model is carried out by using the wind tunnel data with a porous roof model. Finally, a wind tunnel experiment is conducted with scale models of high-rise buildings to measure the external pressures simultaneously at many points on the rooftop or balconies. The internal pressures underneath the decks laid on the rooftop or balconies are computed from the external pressures and the numerical simulation model constructed at the second step. The critical wind speed causing the scattering of decks is predicted, based on the time history of net wind pressures, provided by the difference between the external and internal pressures, and the scattering mechanism obtained in the first step.

2. Wind blow-off test on actual unit flooring decks

2.1. Experimental method and procedure

As mentioned above, the main purpose of this experiment was to discuss the mechanism underlying the scattering of permeable unit flooring decks. For this purpose, a blow-off test with full-scale decks was carried out. Regarding the decks laid on the rooftop of a flat-roofed building, the most critical condition may occur near the windward corner in a cornering wind; this is where large suctions are induced by conical vortices. Such large suctions may be suppressed by parapets (see [2, 10], for example). Since the flooring decks under consideration in the present study are usually used for flat-roofed buildings with 1.1 – 1.2 m high parapets, the above-mentioned cornering winds are not encountered in practice. Therefore, the experiment was carried out for a wind direction normal to the wall. Furthermore, the flow did not simulate the practical condition around the decks.

In the evaluation of scattering wind speeds in Chapter 5, cornering winds are also considered for comparative purposes; the external pressure distributions are measured in Chapter 4. In such a flow condition, the net wind pressure acting on the deck changes both in two directions parallel and perpendicular to the windward wall. However, because the width of the decks was as small as 300 mm (see Fig. 1a), it was assumed that the variation in the direction parallel to the wall could be neglected when predicting the wind speeds which result in scattering. That is, the mechanism for the scattering of decks obtained in this chapter can be used for such a case as tested in Chapter 5.

Fig. 2a shows the experimental set up. Nine actual decks were laid on a testing floor and subjected to strong winds (uniform flow) generated by a blower. The outlet of the blower was 1.0 m wide and 0.9 m high. Two kinds of unit flooring decks, named P3 and P5, were tested. The weight and porosity were respectively 4.53 N and 3.3% for P3 and 4.01 N and 10% for P5. The decks had double cross-shaped slits (see Fig. 1a) and were connected to each other by joints at two points along each perimeter. Therefore, there were slits between two adjacent decks.

The leading edge of the testing floor is schematically illustrated in Fig. 2b. A plate was installed at the leading edge of the testing floor, which acted like a parapet. The height h_p above the testing floor was 0 or 30 mm (equal to the deck height). The distance d between the plate and the leading edge of the first deck was changed from 0 to 300 mm. When $h_p = 0$ mm, the

wind blows into the gap between the decks and the floor; this may generate positive internal pressures, as shown in Fig. 3a. When h_p = 30 mm, on the other hand, the flow separates at the top of the plate, as shown in Fig. 3b. In this case, the decks located near the leading edge were immersed in a separation bubble. Therefore, the flow around the decks and the resultant wind forces acting on the decks were quite different from those for h_p = 0 mm.

It should be mentioned that the purpose of this experiment was not to simulate the practical condition of the flow around the decks but to generate various conditions for discussing the scattering mechanism of the decks. That is, we measured the wind pressures acting on the decks and the critical wind speed that caused the scattering of decks under various conditions. Based on these results, discussion is made of the scattering mechanism.

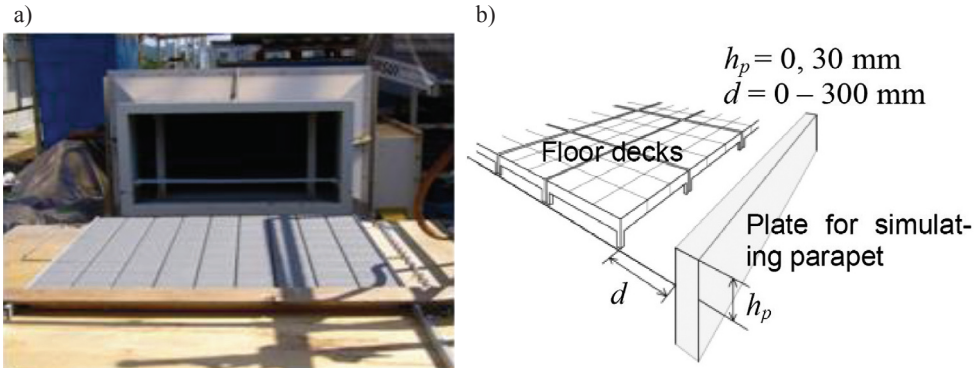

Fig. 2. Experimental setup, a) general view, b) leading edge condition

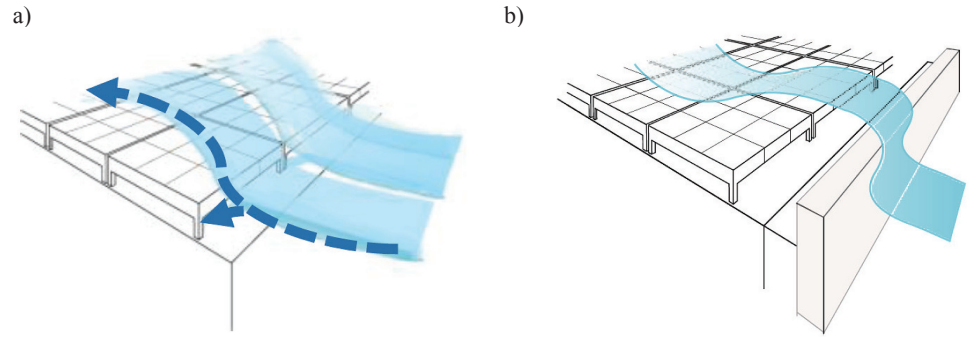

Fig. 3. Flow pattern around flooring decks, a) h_p = 0 mm, b) h_p = 30 mm

Pressure taps of 0.5 mm diameter were installed along the centerline of the deck models and the testing floor. The pressure taps on the testing floor were located just under those on the deck to calculate the net wind pressures acting on the deck, assuming that the pressure on the testing floor was equal to that on the bottom surface of the deck. The pressure taps were connected to pressure transducers in parallel via 100 cm lengths of flexible vinyl tubing with a 1 mm internal diameter. The wind pressures at all taps were sampled simultaneously

at a rate of 200 Hz for 1 min. The compensation for the frequency response of the pneumatic tubing system was carried out in the frequency domain by using the frequency response function of the pressure measuring system. In this experiment, the decks were fixed to the floor so as not to be blown off. Using the time history of the net wind pressures along the centerline, the lift and overturning moment about the leeward edge of the first deck were computed, as shown in Section 2.2.

Next, the critical wind speed U_{cr} (hereafter referred to as 'scattering wind speed') causing the scatter of decks was measured. In this experiment, the decks were loosely laid on the floor. In order to understand the behaviour of decks before scattering, the displacement of the first deck was measured by a laser displacement meter at a point 50 mm downstream from the leading edge.

2.2. Discussion of the scattering mechanism

Figs. 4a and 4b respectively show the time history of displacement of deck (P5) for $h_p = 0$ and 30 mm, as the wind speed U was increased gradually (almost linearly with time); the increasing rate of wind speed was 2 to 3 m/s per minute depending on U_{cr}. The scattering wind speed U_{cr} is presented in the figure. When $h_p = 0$ mm, the decks are raised by the uplift generated by negative external pressure and positive internal pressure (Fig. 4a). At a relatively low wind speed, the decks are blown off almost instantaneously. When $h_p = 30$ mm, on the other hand, the decks start to move up and down (vibrate in the vertical direction) at some wind speed. As the wind speed is increased further, the vibration amplitude increases and finally the decks are blown off at the scattering wind speed U_{cr}. The behaviour of decks is quite different from that for $h_p = 0$ mm. The vibration before scattering may be related to a slower response of the decks to fluctuating wind forces. When $h_p = 0$ mm, once the decks are raised by the uplift, the positive internal pressure is increased by winds blowing into the gap between the decks and the testing floor, generating further increase in the uplift, which in turn raises the decks further. As a result, the decks are blown off almost instantaneously. This behaviour is similar to a divergence. When $h_p = 30$ mm, the decks are immersed in the separation bubble (see Fig. 3b). Therefore, the internal pressure does not change so much even if the decks are raised by the uplift. The decks move up and down according to the fluctuations of wind forces acting on the decks. Such a movement of decks does not affect the flow pattern and the resultant wind forces acting on the decks significantly.

Fig. 5 shows a schematic illustration of the forces acting on the first deck. In the figure, Mg represents the weight of the deck acting on the center of the deck (center of gravity); $C_{p\mathrm{net}}$ represents the net wind pressure coefficient (or pressure difference coefficient), which is a function of the distance x from the leading edge and time t; and L = length of deck (= 300 mm in the present case). The scattering wind speed U_{cr} can be evaluated based on the balance of moments induced by the weight of the deck (counterclockwise) and by the net wind pressure acting on the deck (clockwise) about the trailing edge ($x = 300$ mm) of the first deck. When the moment $m(t)$ induced by the net wind pressure exceeds that by the weight of the deck, the deck will be blown off. Therefore, the scattering wind speed U_{cr} may be given by the following equation:

$$Mg \times \frac{L}{2} = \frac{1}{2}\rho U_{cr}{}^2 \hat{C}_m L^3 \tag{1}$$

where ρ = air density; and $\hat{C}_m$ represents the maximum peak value of the moment coefficient $C_m(t)$ given by the following equation:

$$C_m(t) = \frac{1}{L^2}\int_0^L C_{p\text{net}}(x,t)\cdot\varphi(x)\cdot(L-x)dx \tag{2}$$

where φ(x) is a function representing the effect of a slit on the net wind pressure on the deck; i.e. φ(x) = 0 at the location of slit, while φ(x) = 1 at the other locations. Note that Eq. (2) can be used for square decks with sides L and slits. Kind and Wardlaw [9] proposed a scattering mechanism on the basis of the balance of the lift force and the weight of the deck. Because the application point of the lift is generally different from that of the weight, the scattering mechanism based on the balance of moments seems more reasonable than that based on the balance of vertical forces.

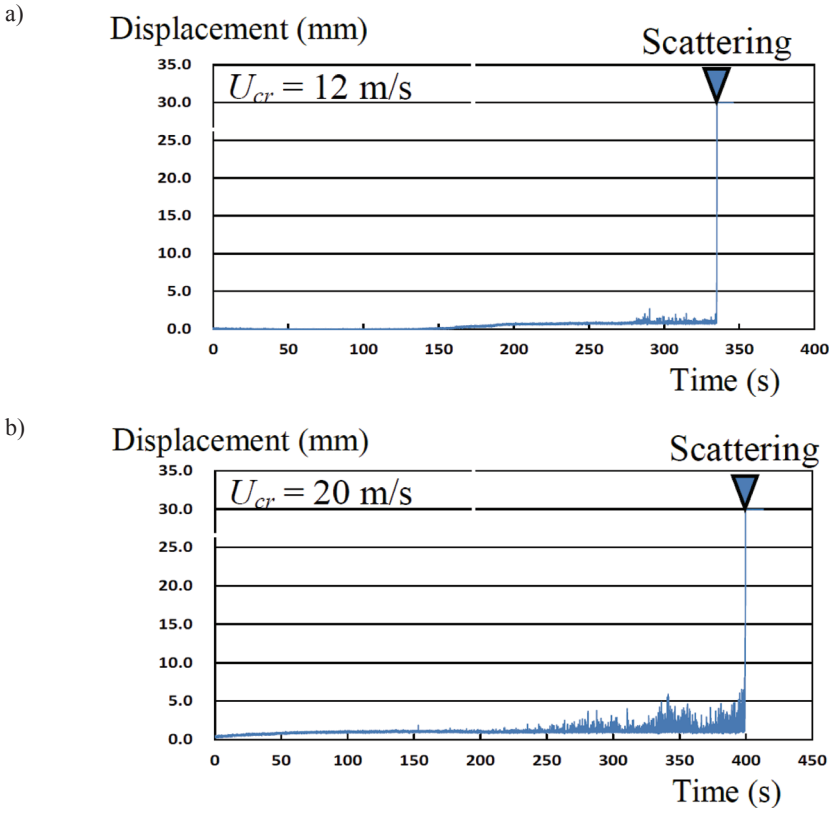

Fig. 4. Time history of displacement of the deck (P5), a) h_p = 0 mm, b) h_p = 30 mm

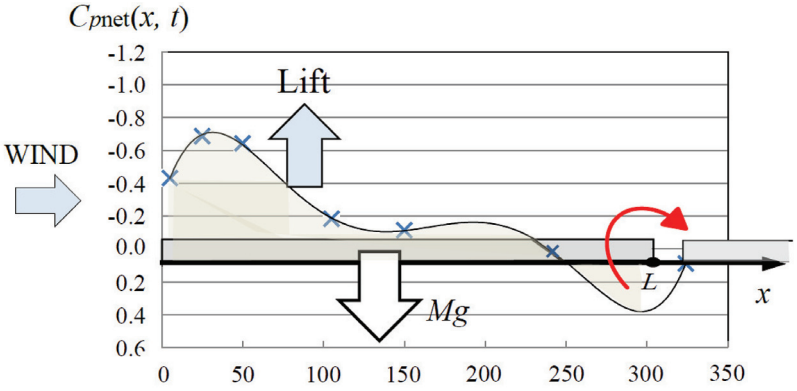

Fig. 5. Deck subjected to wind and gravity forces

The scattering wind speed U_{cr} can be obtained by using the time history of $C_{pnet}(x,t)$. In the calculation, we should consider the difference of the deck's behaviour before scattering, as shown in Fig. 4. This feature may be related to the response of flooring decks to the change in the flow pattern and the resultant wind force acting on the deck, as mentioned above. When $h_p = 0$ mm, the decks are blown off at the moment when Eq. (1) is satisfied. On the other hand, when $h_p = 30$ mm, this is not the case because of the effects of acceleration and damping forces. Such a slow response of the decks to fluctuating wind forces can be considered by applying a moving average to the time history of $C_m(t)$ when evaluating $\hat{C}_m$. Comparing the experimental results on U_{cr} with those predicted by Eq. (1), we found that an averaging time of 1 sec was the most appropriate when $h_p \geq 30$ mm.

Fig. 6 shows a comparison between experimental results and prediction for U_{cr}. A good agreement can be seen in the figure; this implies that the proposed scattering mechanism is reasonable.

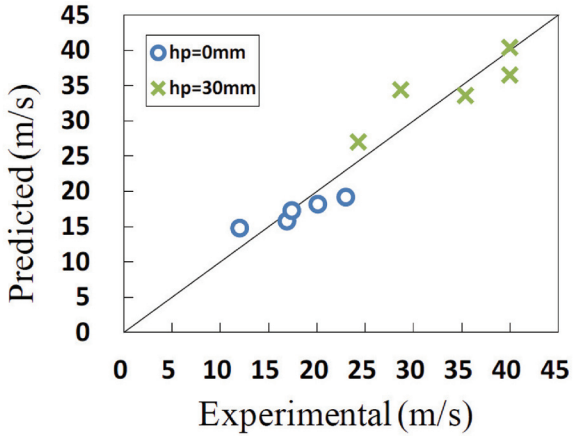

Fig. 6. Comparison between experiment and prediction for scattering wind speed U_{cr}

3. Numerical simulation of internal pressures

3.1. Analytical model of simulation

The internal pressures underneath the decks depend on many factors, such as the external pressures, the gap between adjacent decks and flow resistance underneath the decks. This is identical to the problem of building internal pressure, when the space underneath the deck is regarded as a room in a building [1]. The air flows through the slits or gaps in a vertical direction as well as through the gaps between the adjacent 'rooms' in horizontal directions. The internal pressure is determined from the balance of mass of air flowing into and out of the space underneath each deck. The governing equation of the flow through the gap and/or slit in the deck in the vertical direction (see Figure 7) may be represented by the unsteady Bernoulli equations. The equation for the flow passing through an opening in the vertical direction may be given by the following equations:

$$\rho l_e \frac{dU_e}{dt} = p_e - p_i - \Delta p_1 - \Delta p_2 \tag{3}$$

$$\Delta p_1 = \frac{1}{2} C_{Le} \rho U_e |U_e| \tag{4}$$

$$\Delta p_2 = \lambda \frac{l_e}{d_e} \frac{\rho}{2} U_e |U_e| \tag{5}$$

where l_e = effective depth of the opening; U_e = flow speed in the opening; p_e and p_i represent the external pressure at the opening and the internal pressure, respectively; C_{Le} = pressure loss coefficient of the opening; and λ represents a friction coefficient, which is approximately given by the following equation assuming that the flow through the slit is Hagen-Poiseuille flow:

$$\lambda = 6 \frac{\nu}{U_e d_e} \tag{6}$$

where ν represents the coefficient of kinematic viscosity of the flow. The effective depth l_e may be given by the following equation [18]:

$$l_e = l_0 + 0.89\sqrt{A_e} \tag{7}$$

where l_0 and A_e represent the actual depth and area of the opening, respectively.

Similarly, the governing equation for the flow through the gap between two adjacent 'rooms' in the x direction (see Fig. 7) may be given by the following equation:

$$\rho l_{i,j} \frac{dU_{i+1,j}}{dt} = p_{i,j} - p_{i+1,j} - \frac{1}{2} C_L \rho U_{i+1,j} \left| U_{i+1,j} \right| - \Delta p_{1,x} \tag{8}$$

$$\Delta p_{1,x} = \lambda \frac{L}{d} \frac{\rho}{2} U_{i+1,j} \left| U_{i+1,j} \right| \tag{9}$$

where (i, j) represents the location of the 'room' with i and j being the numbers of the 'room' in the x and y directions, respectively; $l_{i,j}$ = distance from the center of one 'room' to the center of another ; $U_{i+1,j}$ = wind speed in the x direction from 'room' (i, j) to 'room' $(i+1, j)$; $p_{i,j}$ and $p_{i+1,j}$ represent the internal pressures of 'rooms' (i, j) and $(i+1, j)$; and d = height of the 'room'. Similar equations can be obtained for the internal flow in the y direction.

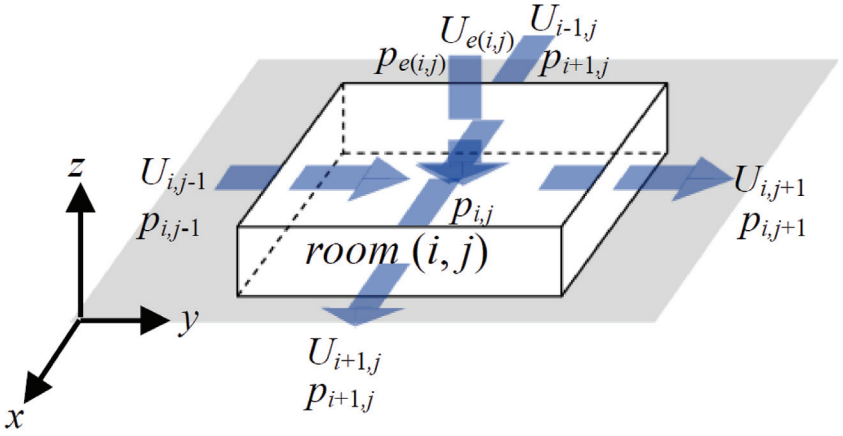

Fig. 7. Schematic illustration of the flow through the slit and gaps

An assumption of weak compressibility of the air and adiabatic condition yields a differential equation that relates the internal pressure to the flow speed through the slits and/or gaps as follows:

$$\frac{dp}{dt} = \frac{\gamma P_0}{V_0} \sum kAU_e \tag{10}$$

where γ = specific heat ratio; P_0 = atmospheric pressure; V_0 = volume of the virtual internal space underneath the deck; k = discharge coefficient; and A = area of the opening.

The non-linear simultaneous equations thus obtained can be solved numerically by using a well-known Runge-Kutta method of the fourth order together with the time history of external pressures obtained from a wind tunnel experiment. The values of parameters involved in the analytical model are calibrated so that the numerical simulation provides results similar to the experimental results, as described in the following section.

3.2. Calibration of the simulation model

The experiments are carried out in a boundary layer wind tunnel with a working section 1.4 m wide, 1.0 m high and 6.5 m long at the Department of Architecture and Building Science, Tohoku University. A turbulent boundary layer with a power law exponent of $\alpha = 0.21$ for the mean wind speed profile is generated on the wind tunnel floor (see Fig. 8). A flat roof model of 360 mm square in cross-section and 60 mm in height is installed in the wind tunnel flow. A 2.5 mm thick plate with many square openings and 36 pressure taps is placed above the roof with a gap of 4 mm, as shown in Fig. 9a. The space underneath the top plate is assumed to be divided into 36 sub-spaces. The area of the openings corresponds to that of the slits and gaps of typical permeable decks. The roof has pressure taps right under the location of the taps on the top plate. The pressure at each tap on the rooftop may represent the internal pressure in each sub-space. The model has parapets along the perimeter, the height (h_p) of which is 6.5 mm or 30 mm. When h_p = 6.5 mm, the top of parapet coincides with the upper level of the 2.5 mm thick permeable plate. The mean wind speed at the roof height H is approximately 10 m/s. The wind direction θ is varied from 0° (normal to a wall) to 45° (parallel to a diagonal). The pressures at 72 taps are low-pass filtered at 300 Hz and then sampled simultaneously at a rate of 400 Hz for a period of 160 sec, from which 16 sets of 10 min data in full scale are obtained.

It should be mentioned that this model is not a scale model of a flat-roofed building on which permeable decks are laid but a virtual model to construct an analytical model for predicting the internal pressures by using the time history of external pressures obtained from a wind tunnel experiment. The statistics of wind pressure coefficients are obtained by applying ensemble average to the results of these 16 consecutive runs.

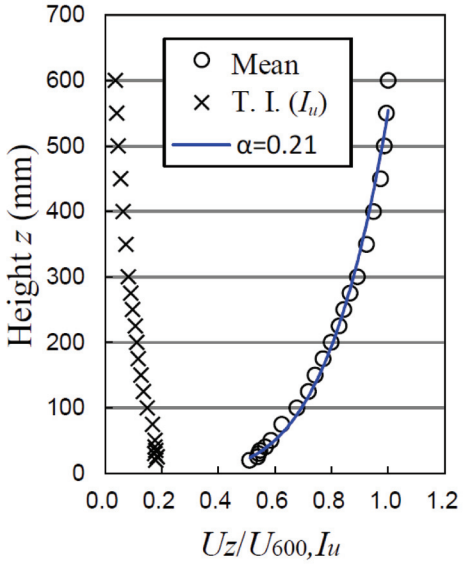

Fig. 8. Profiles of mean wind speed and turbulence intensity

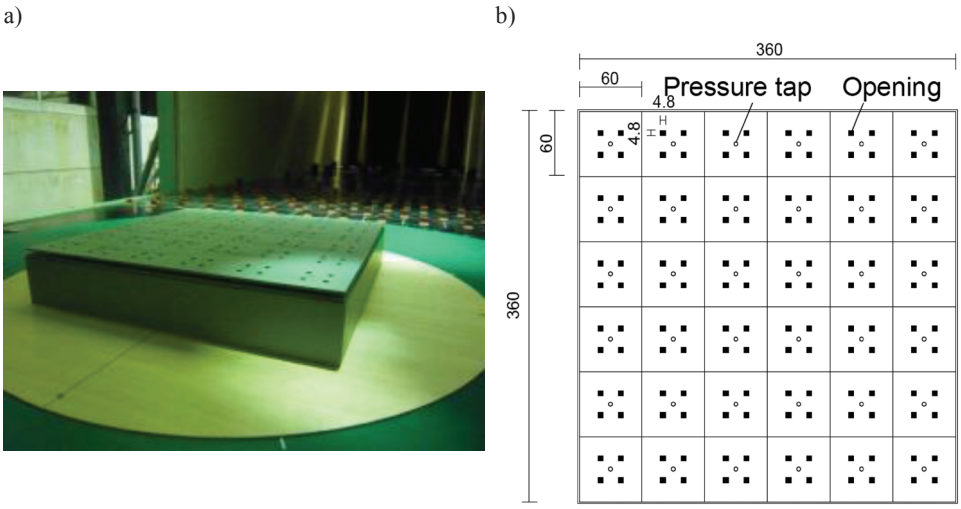

Fig. 9. A flat roof model for the calibration of the analytical model predicting the internal pressures underneath the decks, a) wind tunnel model, b) openings and pressure taps

Because the time step Δt for the pressure measurements is so large for the Runge-Kutta method, a spline function of the 3rd order is applied to the experimental data in order to obtain time history with Δt = 1/4000 s for stable and accurate computations. Furthermore, optimum values of the parameters in the governing equations are determined so that they provide results similar to the experimental results together with theoretical considerations and the results of previous studies. For example, appropriate values of k and C_L are found to be 0.002 and 18.0, respectively.

Figs. 10 to 12 show comparisons between experimental and simulation results for the mean, rms and minimum peak values of internal pressure coefficients, respectively. A relatively good agreement is observed. Similar results were obtained for the other wind directions and for h_p = 30 mm. Therefore, the analytical model will be applied to the decks laid on the rooftop and balconies of buildings in the next chapter.

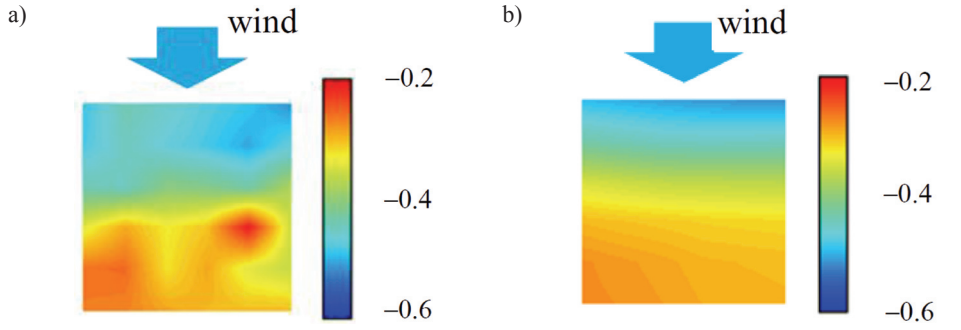

Fig. 10. Comparison between experiment and simulation for the mean internal pressure coefficients (h_p = 6.5 mm, θ = 0°), a) experiment, b) simulation

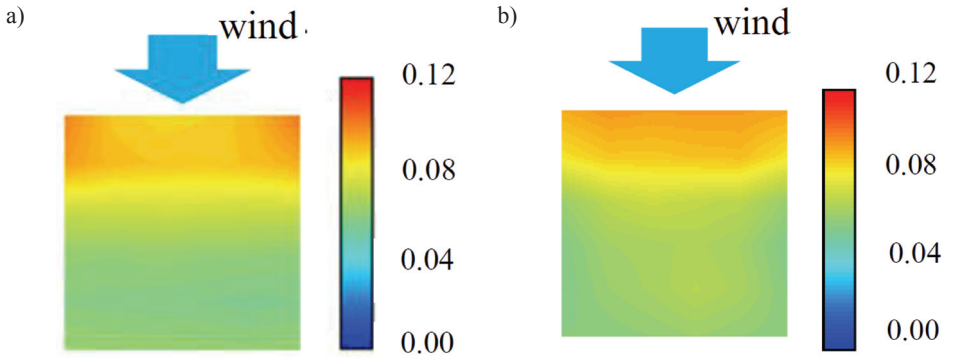

Fig. 11. Comparison between experiment and simulation for the rms internal pressure coefficients (h_p = 6.5 mm, θ = 0°), a) experiment, b) simulation

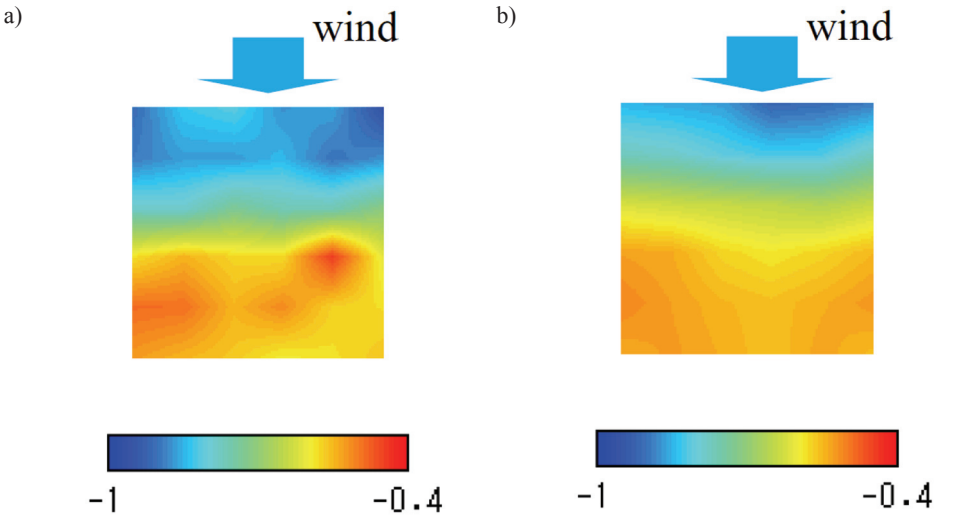

Fig. 12. Comparison between experiment and simulation for the minimum peak internal pressure coefficients (h_p = 6.5 mm, θ = 0°), a) experiment, b) simulation

4. Wind tunnel experiments for measuring external pressures on the rooftops and balconies of buildings

4.1. Experimental procedures

The experiments were carried out in the same wind tunnel flow as that used in Section 3.2. Two models with a geometric scale of λ_L = 1/200 were used; these were called Models A and B, respectively. Model A was a flat roof model with a 10 cm by 10 cm square cross-

section to measure the pressures on the rooftop (Fig. 13a). The aspect ratio H/D of the model was changed from 0.5 to 3.0. Note that not only high-rise but also low-rise and middle-rise buildings were tested in the experiment. The parapet height h_p was changed from 0 to 6 mm (0 to 1.2 m at full scale). As mentioned above, in the case of a flat-roofed building where people can go on the rooftop, the roof generally has parapets 1.1 – 1.2 m high. Even in cases where the balustrade is installed on the parapet (although it is not popular for high-rise buildings), the parapet height is higher than about 0.3 m at full scale. Therefore, lower parapets with $h_p < 0.3$ m are not practical. Many researchers have shown that the parapet affects the negative peak pressure coefficients on the roof significantly. This feature indicates that the parapet affects the scattering wind speed of decks significantly. Therefore, lower parapets were also investigated here for comparative purposes.

Fig. 13b shows the layout of pressure taps on the roof; sixty four taps were drilled on the one quarter area of the roof. The wind direction θ was changed from 0° to 45° at increments of 15°. Model B is a model of 20-story building with balconies (Fig. 14a). Seventy eight pressure taps were drilled on one half of the balcony at the floor, as shown in Fig. 14b. The model consisted of an instrumented part and several dummy parts. Combining these parts in various ways, we measured external pressures on the balconies at the 5th, 10th, 15th and 20th floors. Three kinds of balcony configuration, as shown in Fig. 15, were tested. Note that the *balustrade* type had no walls in the wind tunnel model. The wind direction θ was changed from 0° to 187.5°; i.e. from 0° to 180° at increments of 15° and 187.5°. The pressures at all taps were low-pass filtered at 300 Hz and then sampled simultaneously at a rate of 400 Hz for a period of 160 sec, from which we obtained 16 sets of full-scale 10 min time histories. The statistics of wind pressure coefficients were obtained by applying ensemble average to the results of these 16 consecutive runs in the same manner as that used in Section 3.1.

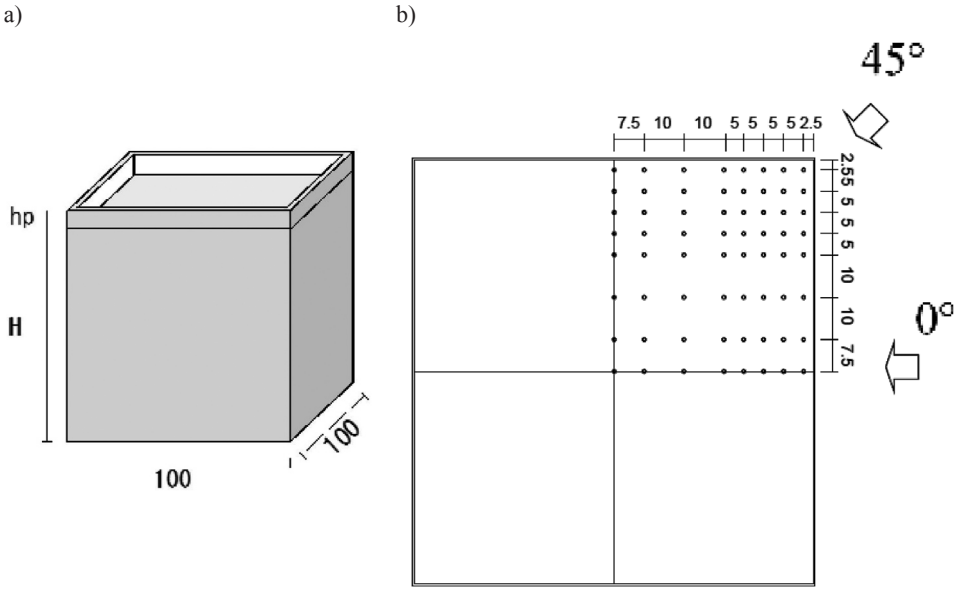

Fig. 13. Flat roof model (Model A), a) general shape, b) layout of pressure taps

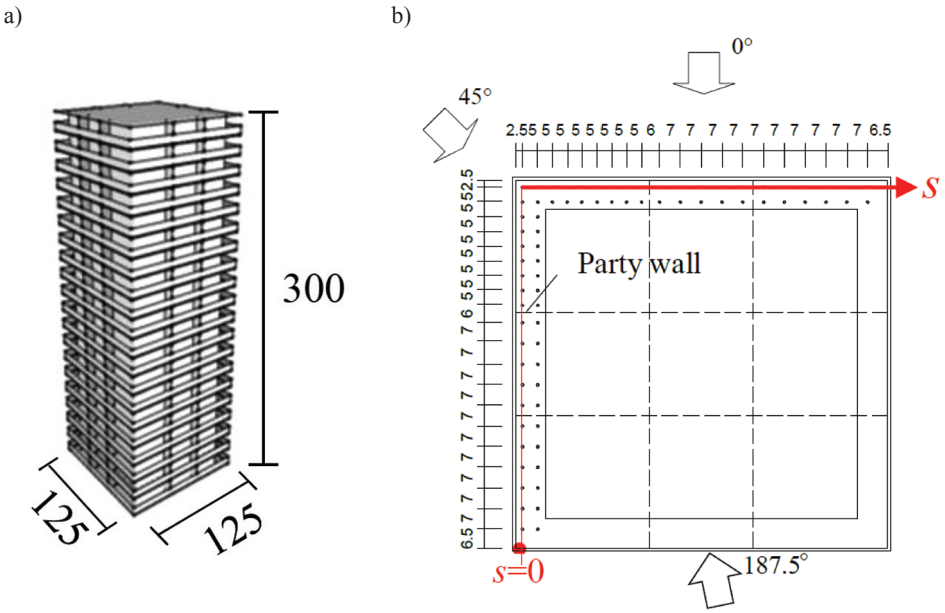

Fig. 14. Model of high-rise building with balconies (Model B), a) general shape, b) layout of pressure taps

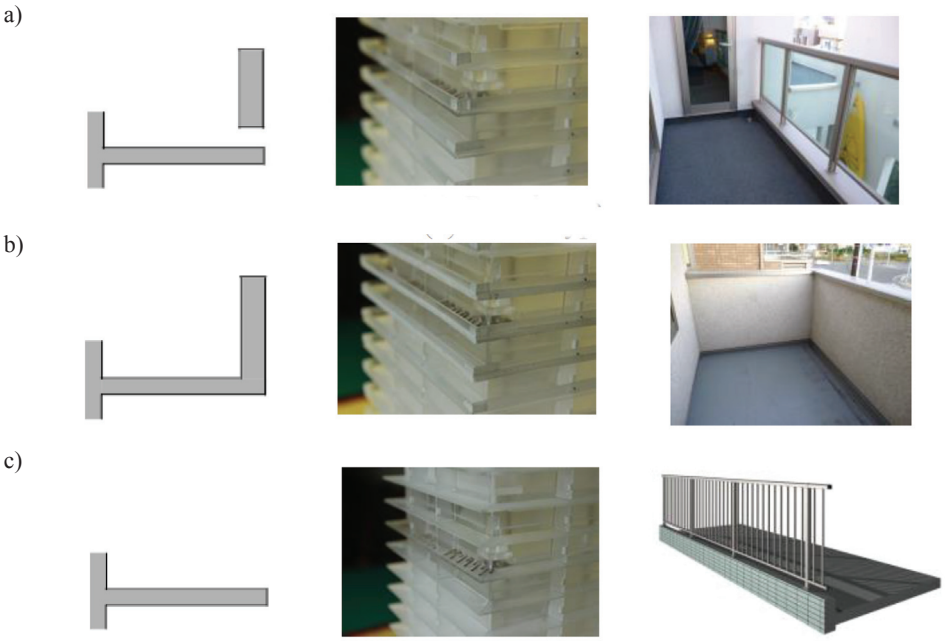

Fig. 15. Balcony configurations tested (Model B), a) *panel* type, b) *spandrel wall* type, c) *balustrade* type

4.2. Experimental results on external pressure coefficients

4.2.1. Pressure distribution on the rooftop of Model A

Fig. 16 shows the effect of h_p on the distribution of the minimum peak pressure coefficients C_{pe_min} on the rooftop of Model A with H = 50 mm. Note that the distribution only in the instrumented area is represented in the figure. As many previous papers (e.g. [8]) have indicated, high peak suctions are induced near the windward corner of the roof without parapets due to the generation of conical vortices in oblique winds (i.e. θ = 30° and 45°). It is interesting to note that the magnitude of negative peak suctions near the corner for h_p = 1 mm is somewhat larger than that for h_p = 0 mm (without parapets). As the parapet height h_p increases further, the magnitude generally decreases, probably due to a longer distance of vortices from the roof surface. The results for h_p = 2 mm, not shown in the present paper to save space, indicate that the negative peak suctions are smaller in magnitude than those for h_p = 0 mm. Further increase in h_p reduces the magnitude of the negative peak suctions, and the distribution becomes more uniform.

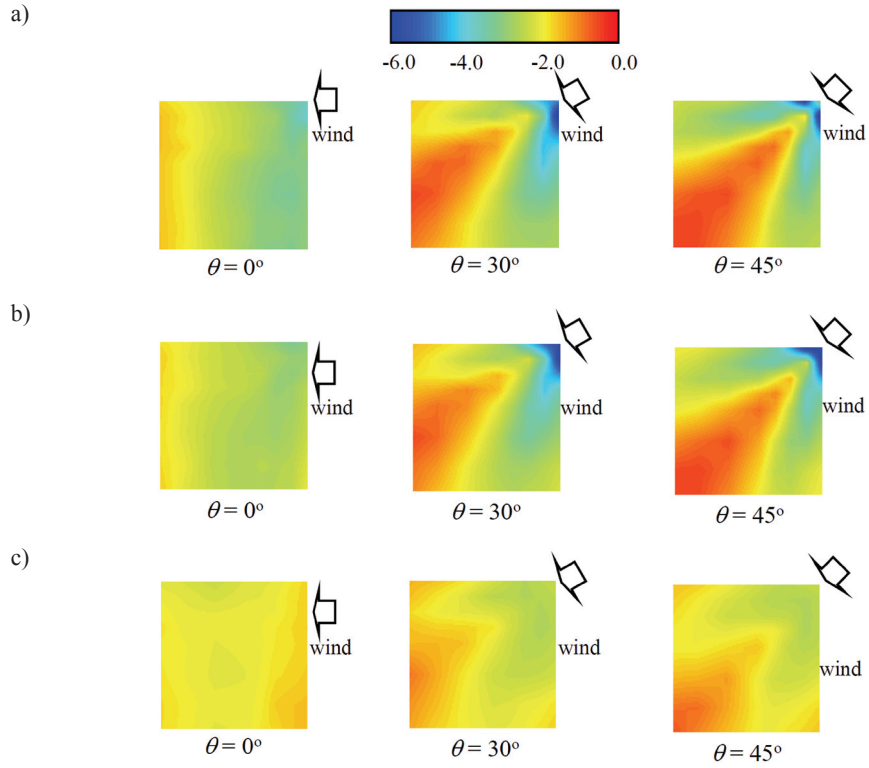

Fig. 16. Distribution of the minimum external peak pressure coefficients C_{pe_min} on the rooftop of Model A with H = 50 mm, a) h_p = 0 mm (0 m in full scale), b) h_p = 1 mm (0.2 m in full scale), c) h_p = 6 mm (1.2 m in full scale)

The results for $H = 300$ mm are shown in Fig. 17. They are qualitatively similar to those in Fig. 16, regarding the effects of h_p and H on the distribution of C_{pe_min}. However, the magnitude of C_{pe_min} is somewhat smaller than that for $H = 50$ mm. This feature may be related to smaller turbulence intensity of the approach flow at the level of the rooftop.

Regarding the effect of parapet height on the negative peak pressure coefficients on the rooftop of low-rise and high-rise buildings, similar features were observed in the previous studies (e.g. [2]). This implies that the present experiment is consistent with the previous ones and the time history of external pressures obtained here can be used for predicting the scattering wind speeds of flooring decks laid on the rooftop of flat-roofed buildings.

The above-mentioned results imply that parapets higher than approximately 30 cm at full scale are effective for preventing the scattering of flooring decks.

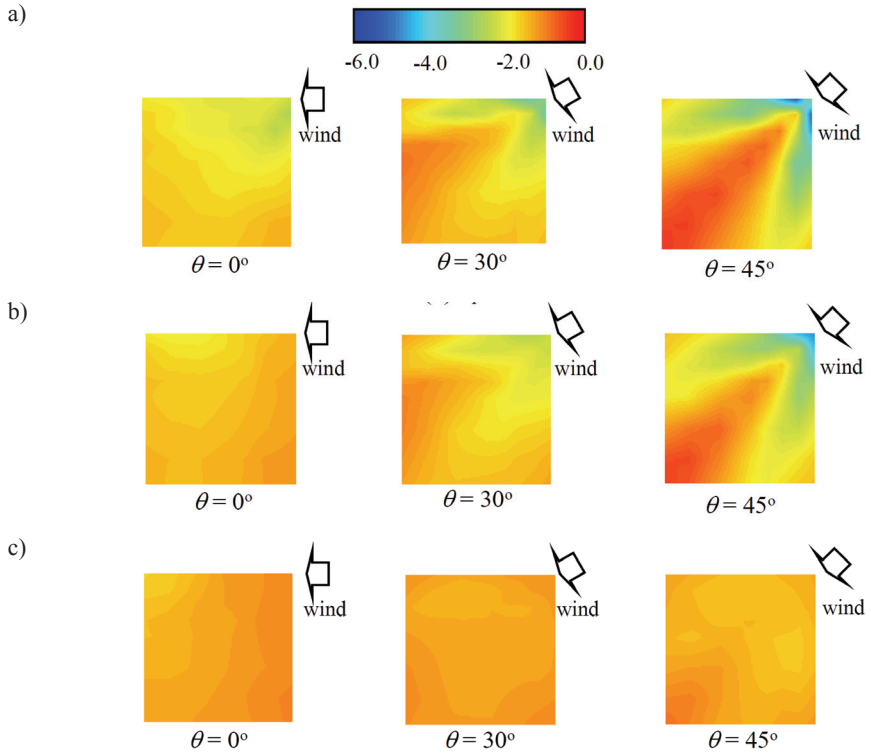

Fig. 17. Distribution of the minimum external peak pressure coefficients C_{pe_min} on the rooftop of Model A with $H = 300$ mm, a) $h_p = 0$ mm, b) $h_p = 1$ mm, c) $h_p = 6$ mm

4.2.2. Pressure distribution on balconies

Figs. 18a and 18b respectively show the distributions of C_{pe_min} along the line passing through the outer pressure taps on the balcony (see Fig. 14b) for *Panel* and *Balustrade*

types, when the wind direction is θ = 0°. In the figures the vertical dashed lines represent the locations of party walls. It is found that the magnitude of C_{pe_min} for the *balustrade* type is generally larger than that for the *panel* type. This feature implies that the *balustrade* type is affected by the separated flow more strongly. The results for the *spandrel wall* type is similar to those for the *panel* type, which means that the gap between the balcony floor and the panel (approximately 10 cm at full scale) minutely affects the external pressures on the balcony.

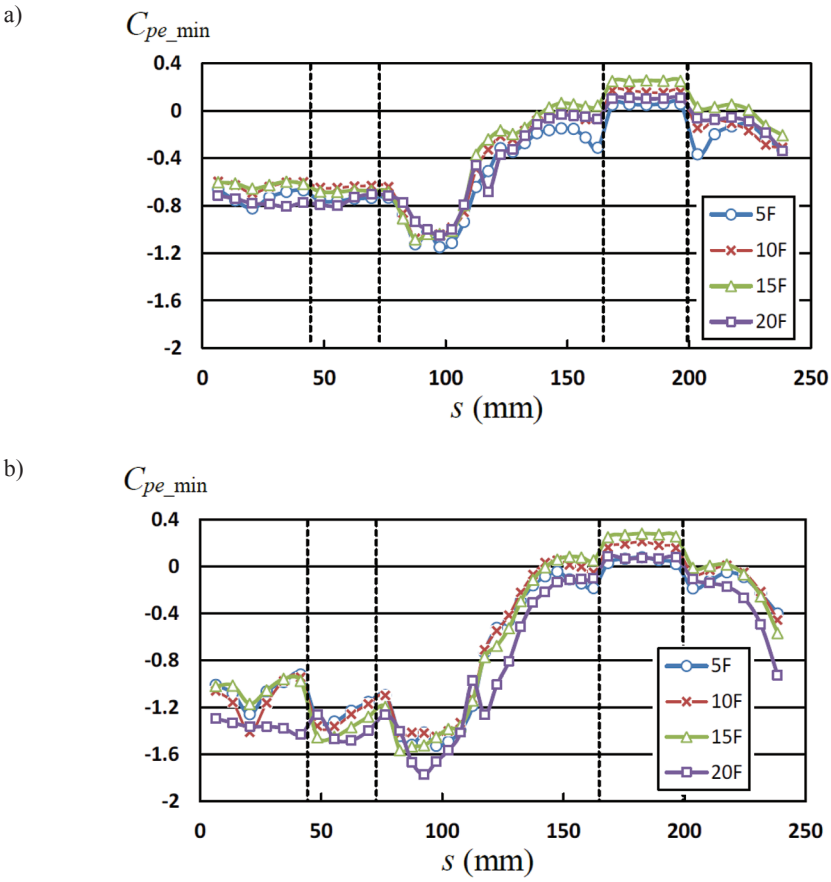

Fig. 18. Distribution of the minimum external peak pressure coefficients C_{pe_min} along the line passing through the outer pressure taps on the balcony of Model B (θ = 0°), a) *panel* type, b) *balustrade* type

The value of C_{pe_min} at each pressure tap changes with wind direction θ significantly. Figure 19 shows the most critical negative peak pressure coefficient at each pressure tap irrespective of wind direction for three balcony types; this may be very important when discussing the scattering of decks. In the figure, the results are represented by coloured circles; each colour represents a range of the pressure coefficient. In the *panel* and *spandrel wall* type cases, larger negative peak values occur near a party wall. The results are similar to

each other. On the other hand, much larger negative peak values are induced in wider areas in the *balustrade* type. Therefore, we should pay much more attention to the scattering of decks in the *balustrade* type.

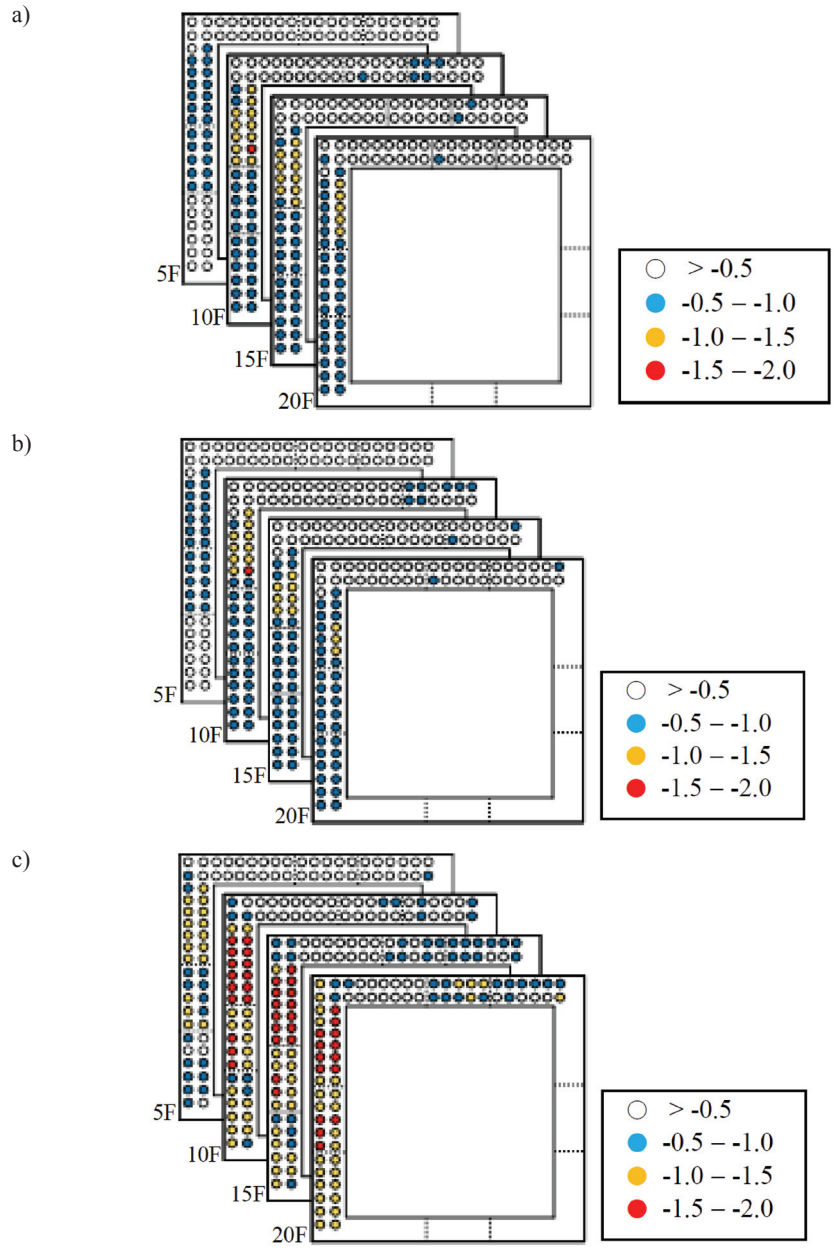

Fig. 19. Most critical negative peak pressure coefficient at each pressure tap irrespective of wind direction, a) *panel* type, b) *spandrel wall* type, c) *balustrade* type

5. Prediction of critical wind speed for the scattering of flooring decks

5.1. Simulated results of internal pressure coefficients

The internal pressures underneath the flooring decks laid on the rooftop or balcony are simulated by using the procedure described in Section 3.1. Fig. 20 shows the distribution of the minimum peak internal pressure coefficients C_{pi_min} on the rooftop of Model A with H = 50 mm when θ = 45°. The results for h_p = 0 and 6 mm are shown in the figure. The distribution of C_{pi_min} looks similar to that of C_{pe_min} (see Fig. 16). The values of C_{pi_min} are generally smaller in magnitude than those of C_{pe_min}, which may be related to the effect of pressure equalization caused by the slits and holes. Similar features are observed for C_{pi_min} on the balconies of high-rise buildings, as shown in Fig. 21. In the figure, the distributions of C_{pi_min} along the line passing through the outer pressure taps on the balcony (*balustrade* type) of Model B are plotted together with that of C_{pe_min}, when the wind direction is θ = 0°.

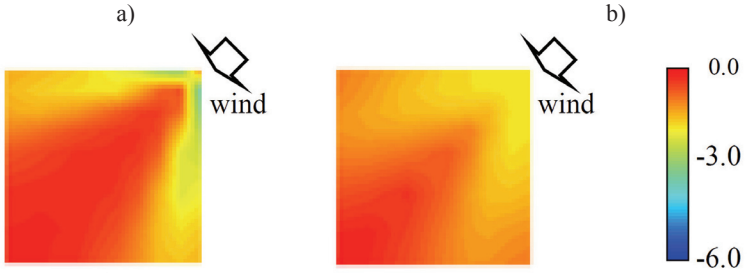

Fig. 20. Distribution of the minimum peak internal pressure coefficients on the rooftop of Model A (H = 50 mm, θ = 45°), a) h_p = 0 mm, b) h_p = 6 mm

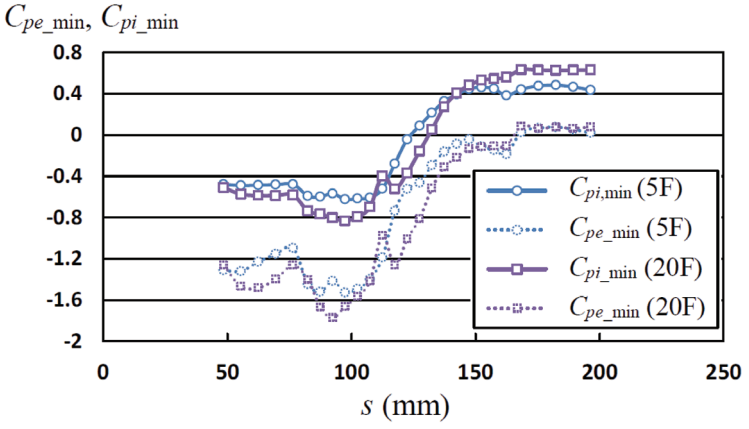

Fig. 21. Distribution of the minimum internal peak pressure coefficients C_{pi_min} along the line passing through the outer pressure taps on the balcony of Model B (θ = 0°)

The procedure for predicting the critical wind speed for the scattering of decks (scattering wind speeds) is as follows. Firstly, the internal pressure coefficients $C_{pi}(x, t)$ underneath the decks are simulated using the time history of external pressure coefficients $C_{pe}(x, t)$ obtained from a wind tunnel experiment. The net wind pressure coefficients $C_{p\text{net}}(x, t)$ on the decks are computed from the time history of $C_{pe}(x, t)$ and $C_{pi}(x, t)$, i.e. $C_{p\text{net}}(x, t) = C_{pe}(x, t) - C_{pi}(x, t)$. Then, the time history of moment coefficient $C_m(t)$ is computed by using Eq. (2). If parapets are installed on the roof or balcony, a moving average of 1 sec in full scale is applied to the time history of $C_m(t)$, from which the peak value $\hat{C}_m$ is obtained. Finally, the scattering wind speed U_{cr} at the level of rooftop H is obtained from Eq. (1) for a given mass M of decks. The value of U_{cr} is the lowest value for all decks and wind directions.

As an example, Table 1 summarizes the predicted values of U_{cr} for the flooring decks when $M = 0.4$ kg.

Table 1

Predicted values of scattering wind speeds U_{cr} for flooring decks (P3) with $M = 0.4$ kg loosely laid on the rooftop of flat-roof buildings and on the balconies of a 20 story building

(a) Rooftop

H (m)	h_p (m)	U_{cr} (m/s)
10	0.0	10.5
	0.2	22.2
	1.2	51.7
20	0.0	11.4
	0.2	26.3
	1.2	57.7
40	0.0	11.8
	0.2	24.1
	1.2	37.1
60	0.0	12.5
	0.2	26.1
	1.2	66.5

(b) Balcony

Type	Floor	U_{cr} (m/s)
Panel	5	35.9
	10	37.6
	15	35.5
	20	34.0
Spandrel wall	5	36.4
	10	36.9
	15	35.5
	20	35.2
Balustrade	5	30.6
	10	28.4
	15	27.0
	20	27.2

6. Concluding remarks

A discussion was made on a prediction model for the critical wind speed causing the scattering of permeable unit flooring decks loosely laid on the rooftop and balconies of high-

rise buildings. This was based on a blowing test, a wind tunnel experiment and a numerical simulation of the internal pressures underneath the decks. In the case of decks laid on the rooftop, the effects of the parapet were considered. Three different types of balcony, which are often used in practice, were considered. The results of a case study indicate that the parapet height significantly affects the scattering wind speeds of decks laid on the rooftop. As the parapet height increases, the scattering wind speed decreases significantly. The balcony type also affects the scattering wind speed of decks. However, the effect is less significant than the parapet height. In general, the *balustrade* type of balcony provides lower scattering wind speeds.

References

[1] Amano T., Fujii K., Tazaki S., *Wind loads on permeable roof-blocks in roof insulation systems*, Journal of Wind Engineering and Industrial Aerodynamics, Vol. 29, 1988, 39-48.

[2] Baskaran A., Stathopoulos T., *Roof corner wind loads and parapet configurations,* Journal of Wind Engineering and Industrial Aerodynamics, Vol. 29, 1988, 79-88.

[3] Bienkiewicz B., Sun Y., *Wind-tunnel study of wind loading on loose-laid roofing systems*, Journal of Wind Engineering and Industrial Aerodynamics, Vol. 41–44, 1992, 1817-1828.

[4] Bienkiewicz B., Sun Y., *Wind loading and resistance of loose-laid roof paver systems*, Journal of Wind Engineering and Industrial Aerodynamics, Vol. 77, 1997, 401-410.

[5] Cheung J.C.K., Melbourne W.H., *Wind loading on a porous roof*, Journal of Wind Engineering and Industrial Aerodynamics, Vol. 29, 1988, 19-28.

[6] Cope A.D., Crandell J.H., Liu Z., Stevig L.J., *Wind loads on fasteners used to attach flexible porous siding on multi-layer wall systems*, Journal of Wind Engineering and Industrial Aerodynamics, Vol. 133, 2014, 150-159.

[7] Gerhardt H.J., Janser F., *Wind loads on wind permeable facades*, Journal of Wind Engineering and Industrial Aerodynamics, Vol. 53, 1994, 37-48.

[8] Kawai H., Nishimura, G., *Characteristics of fluctuating suction and conical vortices on a flat roof in oblique flow*, Journal of Wind Engineering and Industrial Aerodynamics, Vol. 60, 1996, 211-225.

[9] Kind R.J., Wardlaw R.L., *Failure mechanisms of loose-laid roof-insulation systems*, Journal of Wind Engineering and Industrial Aerodynamics, Vol. 9, 1982, 325-341.

[10] Kopp G. A., Surry D., Mans C., *Wind effects of parapets on low buildings: Part 1. Basic aerodynamics and local loads,* Journal of Wind Engineering and Industrial Aerodynamics, Vol. 9, 2005, 817-841.

[11] Kumar, K.S., *Pressure equalization of rain screen walls: a critical review*, Building and Environment, Vol. 35, 2000, 161-179.

[12] Liu H., Saathoff P.J., *Building internal pressure: sudden change*, Journal of Engineering Mechanics Division, ASCE, Vol. 107, 1981, 309-321.

[13] Mooneghi M.A., Irwin P., Chowdhury A.G., *Large-scale testing on wind uplift of roof pavers*, Journal of Wind Engineering and Industrial Aerodynamics, Vol. 128, 2014, 22-36.

[14] Oh J.H., Kopp G.A., Inculet D.R., *The UWO contribution to the NIST aerodynamic database for wind loads on low buildings: Part 3. Internal pressures*, Journal of Wind Engineering and Industrial Aerodynamics, Vol. 95, 2007, 755-779.

[15] Oh J.H., Kopp G.A., *Modeling of spatially and temporally-varying cavity pressures in air-permeable, double-layer roof systems*, Building and Environment, Vol. 82, 2014, 135-150.

[16] Okada H., Ohkuma T., Katagiri J., *Study on estimation of wind pressure under roof tiles*, Journal of Structural and Construction Engineering, Architectural Institute of Japan, Vol. 73, 2008, 1943-1950 (in Japanese).

[17] Trung V., Tamura Y., Yoshida A., *Study on wind loading on porous roof cover sheets on a low-rise building: effects of parapet height and underneath volume*, Proc. 11th Americas Conference on Wind Engineering, San Juan, Puerto Rico 2009.

[18] Vickery B.J., *Gust-factors for internal pressures in low rise buildings*, Journal of Wind Engineering and Industrial Aerodynamics, Vol. 23, 1986, 259-271.